RSC Advances

PAPER

View Article Online
View Journal | View Issue

Cite this: *RSC Adv.*, 2025, **15**, 45909

Modified cellulose-based separator with high transference number and uniform lithium deposition for dendrite-free lithium metal batteries

Chao Gao,†[a] Lianghong Wu,†[b] Yulin Lu,[a] Hang Sun,[a] Yun Li,[a] Weiwei Liu,[a] Jinlan Luo*[c] and Changyong Song *[d]

The demand for high-performance lithium-ion batteries has increased significantly due to the rapid growth of portable electronic devices and new energy vehicles. The separator, an essential component of the battery, directly impacts the safety and cycle performance of the battery. A novel lithium-ion battery separator was fabricated by applying acid-modified halloysite nanotubes (NHNTs) onto cellulose paper (CP). Following the etching process of HNTs using sulfuric acid, the interior cavity of the tubular structure enlarges, creating more pathways for the movement Li^+ ions. This facilitates the even distribution of Li^+ ions and prevents the formation of lithium dendrites. Furthermore, cellulose paper has a significant quantity of hydroxyl groups, which enhances its attraction to the electrolyte. As a result, the NHNTs separator that is produced exhibits exceptional electrolyte absorption rate, commendable thermal stability, and superior mechanical properties. The $LiFePO_4$/NHNTs separator/Li battery has exceptional rate performance, with a charging and discharging capacity of 113 mAh g^{-1} at 5C. Additionally, it demonstrates good cycle performance, maintaining a capacity retention rate of 95.5% after 500 cycles at 1C.

Received 16th September 2025
Accepted 17th November 2025

DOI: 10.1039/d5ra07003a

rsc.li/rsc-advances

1 Introduction

Energy is fundamental to enabling the continued existence and progress of human civilization. Due to the rapid progress of global industrialization and technological advancements, there is a growing need for energy among humans. The extensive use of conventional non-renewable fossil fuels such as coal, oil and natural gas has led to a significant increase in environmental pollution, energy depletion, the greenhouse effect, and other environmental issues. To address these issues, nations worldwide are proactively transforming their energy infrastructure and seeking alternative energy sources to replace conventional fuels.[1–7] Therefore, the development of green renewable clean energy has become an important issue in today's world. The lithium-ion battery is an advanced energy storage device, which has the advantages of environmental friendliness, no memory effect, high specific energy and long cycle life.[4] Widely used in daily life in mobile phones, computers and other portable electronic equipment and new energy vehicles and other fields, it has completely changed the lifestyle and habits of modern people.[8]

The separator is one of the important components of lithium-ion batteries. Although it does not directly participate in the chemical reaction, it can prevent contact between positive and negative electrodes and provide channels for Li^+ to move in the positive and negative electrodes, thus improving the electrochemical performance of lithium-ion batteries.[9–11] However, at present, commercial polyolefin separators have the problem of poor thermal stability, which can easily cause internal short circuiting of the battery and even explosion. Moreover, the wettability between the polyolefin separator and the electrolyte is poor, which is can easily cause the growth of lithium dendrites, and the cycling efficiency is low.[12,13]

Given the issues with commercial separators, researchers have implemented various methods to enhance their performance. The preparation of a lithium-ion battery separator by electrospinning is a common method, and the nanofiber film with porous structure is formed by disorganized arrangements between the fibers, which can improve the porosity and liquid absorption rate of the separator. Yang *et al.*[14] used poly(ethylene oxide) (PEO) as an auxiliary solution, doped benzimidazole in heterocyclic aramid (HA), and prepared a high-performance lithium-ion separator by electrospinning. It not only has high porosity, high electrolyte absorption rate, but it also has

[a]*Shandong Open University, 250014, Jinan, China*
[b]*Jinan Thermoelectric Engineering Co., Ltd, 250022, Jinan, China*
[c]*Center for Advanced Low-Dimension Materials State Key Laboratory for Modification of Chemical Fibers and Polymer Materials, College of Chemistry and Chemical Engineering, Donghua University, Shanghai, 201600, China. E-mail: luojinlan0504@163.com*
[d]*State Key Laboratory of Heavy Oil Processing, School of Materials Science and Engineering, China University of Petroleum (East China), 266580, Qingdao, China. E-mail: songchangyong0515@163.com*
† Chao Gao and Lianghong Wu contributed equally to this work.

excellent flame retardancy, and electrochemical performance has been greatly improved. Li *et al.*[15] first prepared PI nanofiber film by electrospinning, and then formed a tight coating on the surface of PI fiber by using a simple self-adsorption crosslinking technology. The prepared separator had excellent thermal stability, wettability and safety, and the capacity retention rate of 300 cycles at 1C was 82.1%, much higher than that of PP (58.3%). Although the electrospinning process is simple, there are also some problems, such as poor mechanical properties and large pores, which seriously affect the development of separators. Coating the surface of the separator with inorganic nanoparticles is considered as another effective improvement method, that can improve the thermal stability and mechanical properties of the separator.[16,17] Yang *et al.*[18] evenly dispersed Al_2O_3 and cellulose on the separator to build a structure similar to reinforced concrete. The prepared separator showed excellent thermal stability at 200 °C, and its mechanical properties and wettability were greatly improved. Jia *et al.*[19] mixed boehmite nanoparticles with polyvinylidene fluoride–chlorotrifluorinylene (PVDF–CTFE) and fluorinated polyimide (F-PI) to prepare a lithium-ion battery separator by electrospinning and electron beam irradiation. The prepared separators show excellent thermal stability and electrochemical performance, especially improving the cycling performance at high current density, 1000 and 1500 cycles at 10C and 15C, and the capacity retention rate reaches more than 90% and 80%.

Cellulose is one of the most widely distributed and widely used natural biomolecular materials in nature, widely found in plants, algae, marine organisms and bacteria.[20–22] Cellulose is made of glucose groups connected by a 1,4-β glucoside bond, and has a large number of free active hydroxyl groups on the surface, which makes the cellulose molecular chain have a strong hydroxyl interaction.[23] And the cellulose can be modified by etherification,[24] esterification,[25] grafting copolymerization[26] and so on to get different kinds of cellulose to expand its application.[27] Cellulose itself has high thermal stability and chemical stability, in addition, the polar groups on the cellulose molecular chain can increase the affinity with the electrolyte but can also achieve complex with lithium ions, improve the lithium-ion transference number of the separator.[28] Zhu *et al.*[29] prepared a cellulose acetate/polyvinylidene fluoride composite membrane by electrospinning, which was used as a lithium-ion battery separator. The prepared separator had high porosity (76.9%) and excellent thermal stability, and the capacity retention rate was 94.6% after 400 cycles at 5C. Zhang *et al.*[30] prepared a double-layer REDOX active cellulose separator by introducing NiS, which promoted uniform stripping/plating of lithium and inhibited polarization during stripping/plating.

In this study, we successfully coated acid-modified halloysite nanotubes on cellulose paper. The acid-modified halloysite nanotubes (NHNTs) coating improves the separator's mechanical properties and shields it from lithium dendrites impalement. The hollow tube-like structure of NHNTs give Li^+ more ways to move, lowers the impedance of the separator, lets Li^+ be deposited evenly, and makes the cycle performance and rate performance of the separator better. As a result, the $LiFePO_4$ battery assembled by the NHNTs separator showed excellent performance, with a capacity retention rate of 95.5% for 500 cycles at 1C (Scheme 1).

2 Materials and methods

2.1 Materials

Sulfuric acid (H_2SO_4) and *N*-methyl-2-pyrrolidone (NMP) were purchased from Far East Fine Chemical Co., Ltd. Halloysite nanotubes (HNTs) was purchased from Shanghai Mclean Biochemical Technology Co, Ltd. Electrolyte, 1 M $LiPF_6$ in ethylene carbonate (EC)/diethyl carbonate (DEC) (1 : 1, W/W) was bought from Kelude (Guangdong, China). Softwood pulp board was purchased from a factory in Shandong.

2.2 Preparation of cellulose paper

The softwood pulp board was shredded and then soaked in deionized water. Wet paper sheets were prepared from softwood fiber suspensions using a sheet machine former. Then the wet paper sheet was followed by a drying pressing at 100 °C for 10 min. The resulting paper substrate is referred to as CP.

2.3 Etching of HNTs

1.0 g HNTs was evenly distributed in 150 mL sulfuric acid. The mixture was agitated at a temperature of 40 °C for a duration of 36 h. Afterward, the mixture was subjected to centrifugation and rinsed with deionized water until it reached a neutral pH. The resulting solid was then dried in an oven at a temperature of 80 °C overnight. This solid was given the designation NHNTs.

2.4 Preparation of cellulose based lithium ion battery separator

The NHNTs and polyvinylidene fluoride (PVDF, used as a binder) were added to *N*-methylpyrrolidone (NMP) solvent in a mass ratio of 1 : 1, 2 : 1, and 1 : 2. Subsequently, the mixture was stirred at a speed of 300–500 rpm on a magnetic stirrer for 2 hours to ensure complete dissolution of PVDF and the formation of a uniformly dispersed, bubble-free, highly homogeneous slurry. Then, the slurry was evenly coated on both sides of the cellulose paper substrate using a precision coating machine, with the wet film thickness controlled at 10 μm per side to obtain a dense functional coating (total coating area loading of

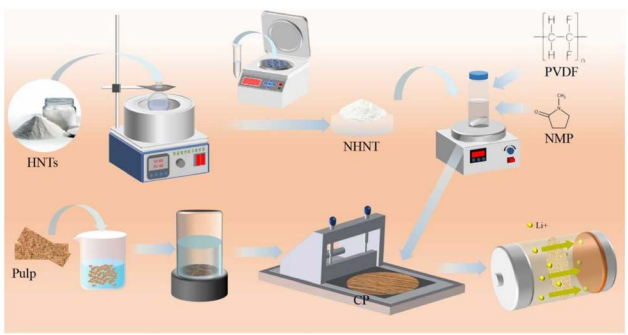

Scheme 1 Schematic diagram of preparation process for the separator.

approximately 2.21 mg cm^{-2}). Finally, the coated composite paper was placed in a vacuum drying oven and dried at 60 °C for 12 hours to completely remove residual solvents and cure the coating.

2.5 Structural and morphological characterizations

The surface of NHNTs was analyzed by XPS (XPS, ESCALABXi). The structure and morphology of NHNTs and separators were observed by scanning electron microscope (SEM, Regulus8820). The thermal stability of NHNTs and separators were analyzed by thermogravimetric analyzer (TGA, TchsGAQ50). Heat the separator in the oven at 50 °C, 100 °C, 150 °C and 200 °C for 30 min to test the thermal shrinkage behavior of the separator. The porosity of the separator was measured by *n*-butanol absorption method. The calculation formula is as follows:[31]

$$\text{Porosity}\% = \frac{W_b - W_a}{\rho_d \times V} \times 100\%$$

where W_b and W_a are the mass of wet separator and dry separator respectively, ρ_d is the density of *n*-butanol, and V is the volume of the dry separator. The absorption rate of the separator was measured by the method of electrolyte absorption. The calculation formula is as follows:[32]

$$\text{Electrolyte uptake }\% = \frac{W_2 - W_1}{W_1} \times 100\%$$

where W_1 and W_2 represent the mass of the dry separator and the separator after absorbing the electrolyte, respectively.

2.6 Electrochemical measurements

The impedance of the separator was measured by the AC impedance method, and the ionic conductivity of the separator was calculated. The calculation formula is as follows:[33]

$$\sigma = \frac{d}{A \times R}$$

where d is the thickness of the separator, A is the contact area, and R is the volume resistance of the separator obtained from the Nyquist plot. The electrochemical stability window of the separators were measured by linear sweep voltammetry, and the scanning range was 0–7 V. The EIS test and *I*–*T* measurement were carried out by electrochemical workstation, and the lithium-ion transference number of the separator was obtained by calculation. The calculation formula is as follows:[16]

$$t_{Li^+} = \frac{I_s(\Delta V - I_0 R_0)}{I_0(\Delta V - I_S R_S)}$$

where I_0 and I_s are the initial and stable current respectively, R_0 and R_s are the initial and polarization resistance respectively. The model 2032 button battery was assembled in a glovebox filled with argon atmosphere, and discharged at 0.1C, 0.2C, 0.5C, 1C, 2C, 5C for 5 cycles at each rate, and then returned to 0.1C rate for 5 cycles to test the rate performance of the battery. The cycle performance of the battery was tested at 1C current density for 500 cycles.

3 Results and discussion

Simple chemical etching of HNTs with sulfuric acid resulted in NHNTs with large internal pores. The results shown in Fig. S1 are similar to HNTs in terms of their XRD properties, which suggests that treating HNTs with acid won't do much damage to their crystal structure. These results are in line with reports in the literature.[34] The thermal stability of HNTs before and after acidification modification was analyzed *via* TGA, and the obtained results are shown in Fig. S2. The thermal degradation curves of HNTs and NHNTs exhibit similarity, suggesting similar thermal stability both before and after modification.[35] The SEM image of HNTs (Fig. S3(a)) revealed a tubular structure that remained unchanged after acidification (Fig. S3(b)). This was primarily caused by the preference of the [AlO_6] octahedral layer on the inner surface of the tubular structure of HNTs to attack under acidic conditions and eliminate Al,[36,37] which was consistent with the XPS image (Fig. S4(c)). Cross section testing of NHNT has been performed with TEM (Fig. S4(a and b)). After acid activation, the hollow tubular structure of halloysite remains unchanged (22 nm), but the inner diameter of the lumen is slightly enlarged (30 nm), and many fine nanoparticles are generated in the lumen.

The synthetic cellulose paper is evenly coated with a layer of NHNTs. In order to obtain a uniform slurry, mix NHNTs and PVDF, add NMP, grind evenly, scrape the resulting slurry evenly on both sides of the cellulose paper, and dry overnight in a 60 °C oven. Fig. 1(a–d) shows the SEM image of the surface of the prepared separator. Compared with the CP separator, the surface of the separator containing NHNTs has a certain amount of porosity, which is caused by the disordered arrangement of NHNTs tubular structures formed during the coating process. At the same time, the existence of these pores promotes electrolyte penetration and improves the separator's ionic conductivity. The EDS data of the NHNTs separator are shown in Fig. 1(e–h). The separator evenly distributed the Si element, confirming a uniform coating of NHNTs on the cellulose paper.

The lithium-ion battery separator should have good thermal stability, which can prevent the separator from shrinking due to high temperature and avoid short circuit caused by contact between positive and negative electrodes.[31] TGA tests were carried out on CP and NHNTs separators, and the experimental results are shown in Fig. 2(a). It can be seen from the figure that

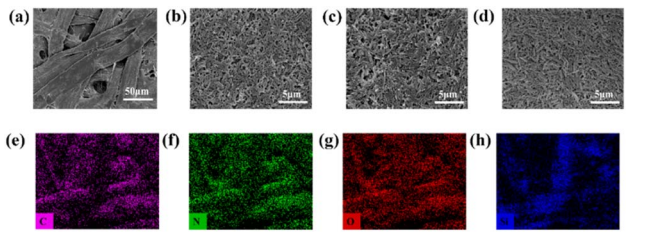

Fig. 1 SEM images of (a) CP, (b) NHNTs 1 : 1, (c) NHNTs 1 : 2, and (d) NHNTs 2 : 1. (e) C energy spectrum of NHNTs, (f) N energy spectrum of NHNTs, (g) O energy spectrum of NHNTs, and (h) Si energy spectrum of NHNTs.

decomposition mainly includes three stages. The first stage is 0–100 °C, which is mainly the weight loss caused by the evaporation of bound and adsorbed water in the separator. The second stage is 100–300 °C, which is mainly due to the weight loss caused by dehydration reaction between cellulose and hydroxyl group in NHNTs. The third stage is 300–450 °C, the weight loss at this stage is mainly from the decomposition of cellulose, but because of the good thermal stability of NHNTs, the composite separator has a higher residual amount at 800 °C.[38] Simultaneously, a qualitative of the separators' thermal stability revealed that the NHNT-containing separator remained unchanged in size and color at up to 200 °C (Fig. S7). In summary, the NHNTs separators have good thermal stability and can reduce the occurrence of thermal runaway phenomenon.

The porosity, absorption rate and wettability of the separator were studied systematically. Fig. 2(b) shows a decrease in the porosity of the separator with NHNTs added, possibly due to NHNTs blocking the CP pores during the coating process. However, the adsorption rate of NHNTs separator increased significantly, which was attributed to the large internal pore of NHNTs modified by acidification and its good affinity with the electrolyte. In Fig. 2(c), the addition of 5 s of electrolyte accelerated the diffusion rate on the NHNTs 2 : 1 separator. The separator's mechanical properties play a crucial role in preventing battery damage due to external force, positive and negative electrode contact, and short circuit phenomenon. Contact angle testing has been measured and electrolyte wetting properties tested. As can be seen from Fig. S6, the acidified electrolyte contact angle is, while the unacidified contact angle is. This may be related to the increase in the specific surface area of nanotubes by acid activation. The separator's mechanical properties underwent testing. Fig. S8 reveals that the CP separator's tensile strength was 20.39 MPa. With the addition of NHNTs, the tensile strength reaches 56.1 MPa, which may be due to the strong interaction between NHNTs and cellulose, as well as hydrogen bond between F atom in PVDF and hydroxyl group in cellulose.[39] In addition, LSV test results show that the separator coated with NHNTs has a wider electrochemical window than CP, which indicates that the separator is practical.

The influence of different temperatures on the ionic conductivity of the separator was tested. The experimental results showed (Fig. 3(a–d)) that the ionic conductivity of the separator gradually increased with the increase in temperature, and the ionic conductivity also gradually increased with the increase of NHNTs content. This is due to the good affinity between NHNTs and the electrolyte, as well as the empty tubular structure of NHNTs, which can provide more ion transport channels. The Arrhenius plots of NHNTs 2 : 1 separator in 25–55 °C was displayed in Fig. S9. The ionic conductivities ($\sigma(T)$) at different temperatures (T) conform to the Arrhenius formula very well: $\sigma(T) = A\exp(-E_a/RT)$, in which E_a is activation energy and A is pre-exponential factor. The NHNTs 2 : 1 separator demonstrated the lowest E_a of 0.04 eV, indicating its faster Li^+ migration. At the same time, the R_{ct} of the separator was also tested, and the impedance variation trend with time within 30 days was also tested and Fig. 3(e–h) displays the experimental results. It can be seen from the figure that the impedance of different separators showed an increasing trend with the increase of time, and the higher the NHNTs content, the slower the increase trend of impedance. In order to further show that the addition of NHNTs is conducive to improving the lithium-ion transfer ability of the separators, the lithium-ion transference number during the charge and discharge of the battery is tested (Fig. 3(i–l)). According to the calculation of the current and resistance before and after polarization, the lithium-ion transference number of the NHNTs separator is 0.69, which is higher than that of the CP separator (0.51). This result is consistent with that of ionic conductivity. Compared with other separators data reported in the literature, the prepared NHNTs separator has certain

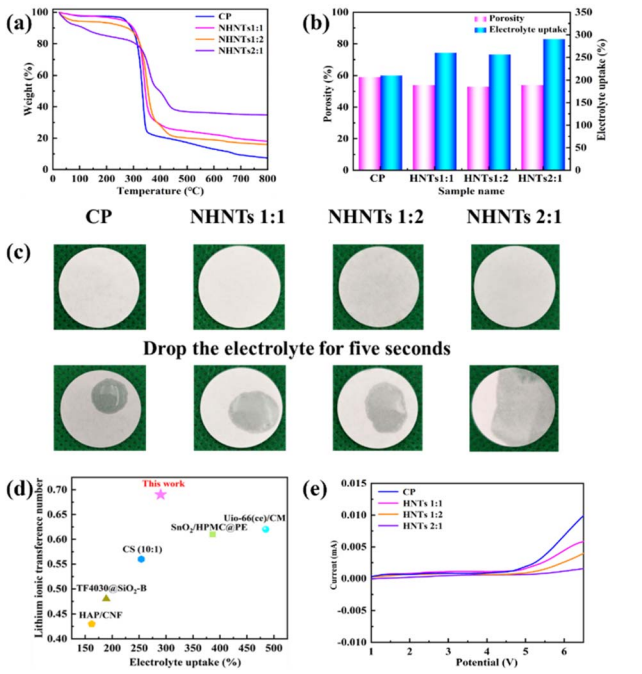

Fig. 2 (a) TGA curves of CP and NHNTs separators; (b) electrolyte uptake and porosity of CP and NHNTs separators; (c) dropping experiments of the electrolyte on CP and NHNTs separators; (d) NHNTs separator comparison of reports on the electrolyte uptake and lithium ion transference number with other separators;[40–44] (e) electrochemical stability window of CP and NHNTs separators.

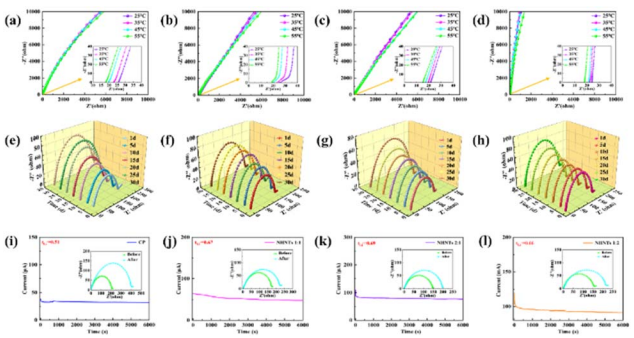

Fig. 3 Nyquist plot for ionic conductivity of (a) CP, (b) NHNTs 1 : 1, (c) NHNTs 2 : 1, (d) NHNTs 1 : 2; R_{ct} evolution of (e) Li/CP/Li, (f) Li/NHNTs 1 : 1/Li, (g) Li/NHNTs 2 : 1/Li, and (h) Li/NHNTs 1 : 2/Li cell with storage time; current–time diagram of (i) CP, (j) NHNTs 1 : 1, (k) NHNTs 2 : 1, (l) NHNTs 1 : 2 and the corresponding Nyquist impedance spectra.

advantages in terms of lithium-ion transference number and electrolyte uptake rate.

In order to further analyze the effect of NHNTs separator on Li^+ migration behavior in the lithium metal anode, the Li//Li symmetrical batteries were assembled, and the effect of NHNTs on the deposition and stripping behavior of lithium metal anode was studied. The experimental results are shown in Fig. 4 and S10. The figure shows that the separator with CP had an initial overpotential of 210 mV in the battery assembly's initial cycle. The polarization voltage increased as time passed, and there were random, irregular voltage oscillations throughout the entire cycle. This showed that the electrolyte in the separator was always being used up, and dead lithium was being made and deposited. This results in an increase in impedance, ultimately leading to the uncontrolled growth of lithium dendrites.[45] The battery with the NHNTs separator, on the other hand, can keep its low potential voltage of 70 mV throughout the 2000 h cycle. This shows that the NHNTs can make the Li^+ distribution more even and effectively stop the growth of lithium dendrites. In addition, the symmetric cycling of Li/Li symmetric batteries with NHNTs 2 : 1 separators at different current densities was tested, and the results were shown in Fig. S10(c). As shown, NHNTs 2 : 1 separators exhibit unusually stable voltage profiles and overpotentials at different current densities. There was no sign of voltage noise or failure, which is an early indicator of dendrite formation and unstable cycling. Furthermore, we analyzed the morphology of lithium metal following a Li/Li symmetrical battery cycle. After cycling the CP separator, the surface of the lithium metal was rough and lithium dendrites formed. On the other hand, after cycling the separator with NHNTs added, the surface of the lithium metal was mostly smooth (Fig. S11), which was in line with the results of the symmetric battery interface performance test.

Subsequently, the $LiFePO_4$/separator/Li half battery was constructed to conduct a rate performance test. The charge and discharge capacities were measured at current densities of 0.1C, 0.2C, 0.5C, 1C, 2C and 5C. Following this, the battery underwent 5 cycles, with cycle later returning to a current density of 0.1C. The discharge capacity of the CP separator and NHNTs separators is the same at 0.1C, reaching 152 mAh g^{-1}. This information is presented in Fig. 4(b) and S12. As the current density increase, the discharge capacity of CP separator decreases more rapidly. At 5C, the battery's capacity is 101 mAh g^{-1}, however the battery's capacity, when built with NHNTs separator, reaches 113 mAh g^{-1}. Upon comparing the battery data of CP separator with the NHNTs separator, it is evident that the NHNTs-coated separator exhibits superior charge and discharge capacity when subjected to high current density. Ultimately, the battery's cycle performance was evaluated by testing, as shown in Fig. 4(c). After undergoing 500 cycles with a current density of 1C, the battery that used the CP separator retained 90.9% of its capacity. On the other hand, the battery that used the NHNTs separator retained 95.5% of its capacity and achieved a Coulomb efficiency of almost 100% after the same number of cycles. The performance of NHNTs diaphragm cell in terms of cycle is superior to that of CP diaphragm cell. The exceptional cycling performance demonstrates that the hollow tubular structure of NHNTs facilitates increased Li^+ transport channels, resulting in a uniform deposition of Li. The alterations in the morphological of lithium metal following cycling were observed (Fig. S13). After cycling with a CP separator, the surface of lithium metal exhibited the presence of small particles. In contrast, while using NHNTs separator, the surface of lithium metal remained reasonably smooth and flat.

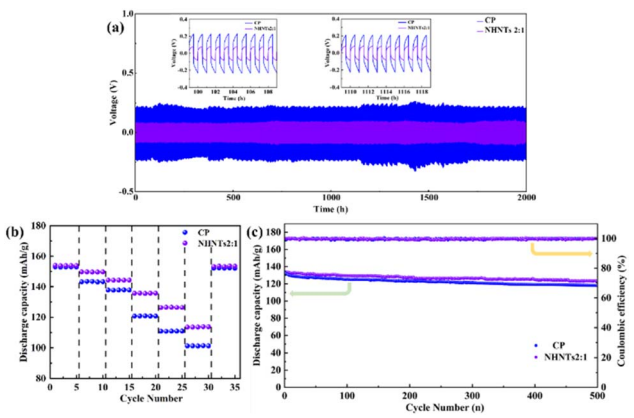

Fig. 4 (a) Voltage *versus* time plots symmetric cell under a current density of 0.1 mA cm^{-2}; (b) C-rate capability; (c) cycling performance at 1C.

4 Conclusions

To prepare a lithium-ion battery separator, we etched the inner wall of HNTs with sulfuric acid and coated it on CP paper. The NHNTs' widened cavity can provide more transmission channels for Li^+, increase the transmission capacity of Li^+, and allow uniform deposition of Li, which stops the growth of lithium dendrites. The separator made from NHNTs and CP has excellent wettability and electrolyte absorption. The assembled Li/Li symmetric battery can maintain a low overpotential voltage at 2000 h, and the capacity retention rate of $LiFePO_4$ battery is as high as 95.5% after 500 cycles at 1C current density. As a result, this study developed a simple method for making a green, pollution-free bio-based lithium-ion battery separator, which has significant advantages in inhibiting the growth of lithium dendrites and improving the battery cycle performance. Building upon these promising results, future work will focus on extending the application of this separator to other advanced battery systems—such as high-energy-density lithium–metal batteries (*e.g.*, with NCM811 cathodes) and lithium–sulfur batteries—to further validate its universal practicality and performance benefits.

Author contributions

Chao Gao: writing original draft, investigation, data curation, funding acquisition; Lianghong Wu: supervision, resources, project administration, investigation; Yulin Lu: software; Hang Sun: conceptualization; Jinlan Luo: supervision, investigation; Changyong Song: writing: review & editing.

Conflicts of interest

There are no conflicts to declare.

Data availability

Data will be made available on request.

Supplementary information (SI): experimental details. See DOI: https://doi.org/10.1039/d5ra07003a.

Acknowledgements

This investigation was supported by Shandong Open University 2024 Special Project (2024108KZ), Shandong Open University 2024 Special Project (2024004JZ).

References

1 D. Larcher and J. M. Tarascon, Towards greener and more sustainable batteries for electrical energy storage, *Nat. Chem.*, 2014, **7**(1), 19–29, DOI: 10.1038/nchem.2085.

2 M. Li, J. Lu, Z. Chen and K. Amine, 30 Years of Lithium-Ion Batteries, *Adv. Mater.*, 2018, **30**(33), 1800561, DOI: 10.1002/adma.201800561.

3 Z. Zhu, T. Jiang, M. Ali, Y. Meng, Y. Jin, Y. Cui and W. Chen, Rechargeable Batteries for Grid Scale Energy Storage, *Chem. Rev.*, 2022, **122**(22), 16610–16751, DOI: 10.1021/acs.chemrev.2c00289.

4 R. Wang, Y. Liu, Q. Luo, P. Xiong, X. Xie, K. Zhou, W. Zhang, L. Zhang, H. J. Fan and C. Zhang, Remolding the Interface Stability for Practical Aqueous Zn/I2 Batteries *via* Sulfonic Acid-Rich Electrolyte and Separator Design, *Adv. Mater.*, 2025, **37**(16), 2419502, DOI: 10.1002/adma.202419502.

5 Z. Liu, S. Chen, Z. Shi, P. Qiu, K. He, Q. Lu, M. Yu and T. Liu, Multivalent Dipole Interactions-Driven Supramolecular Polymer Layer Enables Highly Stable Zn Anode Under Harsh Conditions, *Adv. Energy Mater.*, 2025, **15**(29), 2502010, DOI: 10.1002/aenm.202502010.

6 Z. Liu, L. Sun, X. Liu and Q. Lu, Stabilization Strategies of Lithium Metal Anode Toward Dendrite-Free Lithium-Sulfur Batteries, *Chem.–Eur J.*, 2024, **30**(60), e202402032, DOI: 10.1002/chem.202402032.

7 W. Zhang, Q. Lu, G. Sun, Z. Chen, P. Yue, G. Zhang, B. Song and K. Song, Sodiophilic Interface Induces a NaF-Rich Solid Electrolyte Interface for Stable Sodium–Metal Batteries under Harsh Conditions, *Nano Lett.*, 2025, **25**(15), 6092–6100, DOI: 10.1021/acs.nanolett.4c06612.

8 A. Yoshino, The Birth of the Lithium-Ion Battery, *Angew. Chem., Int. Ed.*, 2012, **51**(24), 5798–5800, DOI: 10.1002/anie.201105006.

9 J. Dai, C. Shi, C. Li, X. Shen, L. Peng, D. Wu, D. Sun, P. Zhang and J. Zhao, A rational design of separator with substantially enhanced thermal features for lithium-ion batteries by the polydopamine–ceramic composite modification of polyolefin membranes, *Energy Environ. Sci.*, 2016, **9**(10), 3252–3261, DOI: 10.1039/c6ee01219a.

10 K. J. Kim, J.-H. Kim, M.-S. Park, H. K. Kwon, H. Kim and Y.-J. Kim, Enhancement of electrochemical and thermal properties of polyethylene separators coated with polyvinylidene fluoride–hexafluoropropylene co-polymer for Li-ion batteries, *J. Power Sources*, 2012, **198**, 298–302, DOI: 10.1016/j.jpowsour.2011.09.086.

11 C. Zhu, J. Zhang, J. Xu, X. Yin, J. Wu, S. Chen, Z. Zhu, L. Wang and H. Wang, Facile fabrication of cellulose/polyphenylene sulfide composite separator for lithium-ion batteries, *Carbohydr. Polym.*, 2020, **248**, 116753, DOI: 10.1016/j.carbpol.2020.116753.

12 H. Lee, M. Yanilmaz, O. Toprakci, K. Fu and X. Zhang, A review of recent developments in membrane separators for rechargeable lithium-ion batteries, *Energy Environ. Sci.*, 2014, **7**(12), 3857–3886, DOI: 10.1039/c4ee01432d.

13 S. S. Zhang, A review on the separators of liquid electrolyte Li-ion batteries, *J. Power Sources*, 2007, **164**(1), 351–364, DOI: 10.1016/j.jpowsour.2006.10.065.

14 S. Yang, M. Zhao, R. He, Y. Chen, Y. Guo, H. Wang, Z. Wang, T. Qiu and X. Tuo, Solution Blow Spinning of the Benzimidazole-Containing Aramid Nanofibers for Separators of Lithium-Ion Batteries, *ACS Appl. Mater. Interfaces*, 2024, **16**(12), 15362–15371, DOI: 10.1021/acsami.4c00902.

15 X. Li, K. Liu, N. Dong, B. Liu, G. Tian, S. Qi and D. Wu, A dendrite-blocking polyimide-meta-aramid separator with ultrahigh strength and thermostability for high-security lithium-ion battery, *Chem. Eng. J.*, 2024, **481**, 148525, DOI: 10.1016/j.cej.2024.148525.

16 H. Sun, Z. Liu, X. Sang, R. Li, P. Li and X. Hu, Mechanically Robust and Safe Separators Based on Inorganic Nanofibers for Lithium-Ion Batteries, *ACS Appl. Energy Mater.*, 2024, **7**(13), 5537–5547, DOI: 10.1021/acsaem.4c01093.

17 L. Wang, Y. Wang, J. Yang, F. Quan, B. Wang, L. Shao, L. Tan, X. Tian and Y. Xia, An eco-friendly and flame-retardant bio-based fibers separator with fast lithium-ion transport towards high-safety lithium-ion batteries, *J. Power Sources*, 2024, **613**, 234950, DOI: 10.1016/j.jpowsour.2024.234950.

18 Z. Yang, L. Chen, J. Xue, M. Su, F. Zhang, L. Ding, S. Wang and H. Wang, Nano-alumina@cellulose-coated separators with the reinforced-concrete-like structure for high-safety lithium-ion batteries, *Chin. J. Chem. Eng.*, 2024, **68**, 83–93, DOI: 10.1016/j.cjche.2023.07.015.

19 S. Jia, S. Yang, Y. Pan, S. U. Din and Y. Cai, Boehmite-PVDF-CTFE/F-PI composite separator irradiated by electron beam for high-rate lithium-ion batteries, *J. Membr. Sci.*, 2024, **704**, 122827, DOI: 10.1016/j.memsci.2024.122827.

20 M. Zhou, D. Chen, Q. Chen, P. Chen, G. Song and C. Chang, Reversible Surface Engineering of Cellulose Elementary Fibrils: From Ultralong Nanocelluloses to Advanced Cellulosic Materials, *Adv. Mater.*, 2024, **36**(21), 2312220, DOI: 10.1002/adma.202312220.

21 K. Li, C. M. Clarkson, L. Wang, Y. Liu, M. Lamm, Z. Pang, Y. Zhou, J. Qian, M. Tajvidi, D. J. Gardner, *et al.*, Alignment of Cellulose Nanofibers: Harnessing Nanoscale Properties to Macroscale Benefits, *ACS Nano*, 2021, **15**(3), 3646–3673, DOI: 10.1021/acsnano.0c07613.

22 M. N. Azman Mohammad Taib, T. S. Hamidon, Z. N. Garba, D. Trache, H. Uyama and M. H. Hussin, Recent progress in cellulose-based composites towards flame retardancy

applications, *Polymer*, 2022, **244**, 124677, DOI: 10.1016/j.polymer.2022.124677.

23 R. J. Moon, A. Martini, J. Nairn, J. Simonsen and J. Youngblood, Cellulose nanomaterials review: structure, properties and nanocomposites, *Chem. Soc. Rev.*, 2011, **40**(7), 3941–3994, DOI: 10.1039/c0cs00108b.

24 J. You, X. Zhang, Q. Mi, J. Zhang, J. Wu and J. Zhang, Mild, rapid and efficient etherification of cellulose, *Cellulose*, 2022, **29**(18), 9583–9596, DOI: 10.1007/s10570-022-04879-x.

25 J. A. Ávila Ramírez, E. Fortunati, J. M. Kenny, L. Torre and M. L. Foresti, Simple citric acid-catalyzed surface esterification of cellulose nanocrystals, *Carbohydr. Polym.*, 2017, **157**, 1358–1364, DOI: 10.1016/j.carbpol.2016.11.008.

26 S. Zhao, J. Li, L. Wu, M. Hua, C. Jiang, Y. Pan, L. Yao, S. Xu, J. Ge and G. Pan, Synthesis and Characterization of Cellulose Diacetate-Graft-Polylactide *via* Solvent-Free Melt Ring-Opening Graft Copolymerization, *Polymers*, 2022, **15**(1), 143, DOI: 10.3390/polym15010143.

27 A. Carlmark, E. Larsson and E. Malmström, Grafting of cellulose by ring-opening polymerisation – A review, *Eur. Polym. J.*, 2012, **48**(10), 1646–1659, DOI: 10.1016/j.eurpolymj.2012.06.013.

28 Z. Liu, R. Wang, Q. Ma, H. Kang, L. Zhang, T. Zhou and C. Zhang, Application of cellulose-based hydrogel electrolytes in flexible batteries, *Carbon Neutralization*, 2022, **1**(2), 126–139, DOI: 10.1002/cnl2.20.

29 Z. Zhu, X. Shi, J. Zhou, X. Li, Y. Liu, Y. Li, Y. Xiong and Y. Zhu, A gel polymer electrolyte obtained from cellulose acetate/polyvinylidene fluoride composite electrospun membrane for safe lithium metal batteries with high-rate capability, *Polymer*, 2024, **308**, 127412, DOI: 10.1016/j.polymer.2024.127412.

30 Y. Zhang, W. Du, D. Ye, J. Zhou, W. Xu and J. Xu, Redox-active NiS@bacterial cellulose nanofiber composite separators with superior rate capability for lithium-ion batteries, *Int. J. Biol. Macromol.*, 2024, **268**, 131622, DOI: 10.1016/j.ijbiomac.2024.131622.

31 X. Song, X. Lei, T. Tian, T. Yu, H. Zhu, Z. Zhang, G. Li, X. Xu and Z. Wang, Constructing 3D porous network channel on PP-based separator to achieve homogeneous deposition of lithium ions for lithium metal battery, *Electrochim. Acta*, 2024, **499**, 144568, DOI: 10.1016/j.electacta.2024.144568.

32 J. Li, L. Lu, H. Liang, Y. Sun, X. Guo, Z. Wei and Y. Zhao, Silkworm cocoon-inspired and robust nanofibrous composite separator with gradient structure for lithium ion batteries, *Compos. Struct.*, 2024, **339**, 118161, DOI: 10.1016/j.compstruct.2024.118161.

33 C. Gao, X. Li, C. Song, G. Wei, X. Zhao, S. Wang and F. Kong, Electrospun polyimide/cellulose acetate propionate nanofiber membrane-based gel polymer electrolyte with fast lithium-ion transport and high interface stability for lithium metal batteries, *Cellulose*, 2023, **30**(14), 9113–9126, DOI: 10.1007/s10570-023-05434-y.

34 D. Garcia-Garcia, J. M. Ferri, L. Ripoll, M. Hidalgo, J. Lopez-Martinez and R. Balart, Characterization of selectively etched halloysite nanotubes by acid treatment, *Appl. Surf. Sci.*, 2017, **422**, 616–625, DOI: 10.1016/j.apsusc.2017.06.104.

35 W. Wang, A. C. Y. Yuen, Y. Yuan, C. Liao, A. Li, I. I. Kabir, Y. Kan, Y. Hu and G. H. Yeoh, Nano architectured halloysite nanotubes enable advanced composite separator for safe lithium metal batteries, *Chem. Eng. J.*, 2023, **451**, 138496, DOI: 10.1016/j.cej.2022.138496.

36 Y. Li, X. Yuan, L. Jiang, H. Dai, Y. Zhao, X. Guan, J. Bai and H. Wang, Manipulation of the halloysite clay nanotube lumen for environmental remediation: a review, *Environ. Sci.: Nano*, 2022, **9**(3), 841–866, DOI: 10.1039/d1en01032h.

37 V. Bertolino, G. Cavallaro, S. Milioto and G. Lazzara, Polysaccharides/Halloysite nanotubes for smart bionanocomposite materials, *Carbohydr. Polym.*, 2020, **245**, 116502, DOI: 10.1016/j.carbpol.2020.116502.

38 D. Verma, M. Okhawilai, N. Senthilkumar, K. Subramani, A. Incharoensakdi, G. G. Raja and H. Uyama, Augmentin loaded functionalized halloysite nanotubes: A sustainable emerging nanocarriers for biomedical applications, *Environ. Res.*, 2024, **242**, 117811, DOI: 10.1016/j.envres.2023.117811.

39 A. A. Issa, M. Al-Maadeed, A. S. Luyt, M. Mrlik and M. K. Hassan, Investigation of the physico-mechanical properties of electrospun PVDF/cellulose (nano)fibers, *J. Appl. Polym. Sci.*, 2016, **133**(26), 43594, DOI: 10.1002/app.43594.

40 X. Zeng, Y. Liu, R. He, T. Li, Y. Hu, C. Wang, J. Xu, L. Wang and H. Wang, Tissue paper-based composite separator using nano-SiO2 hybrid crosslinked polymer electrolyte as coating layer for lithium ion battery with superior security and cycle stability, *Cellulose*, 2022, **29**(7), 3985–4000, DOI: 10.1007/s10570-022-04499-5.

41 Y. Liu, C. Li, C. Li, Z. Liang, X. Hu, H. Liu, Z. Zhang, M. Cui, G. Chen, J. Wan, *et al.*, Highly Thermally Stable, Highly Electrolyte-Wettable Hydroxyapatite/Cellulose Nanofiber Hybrid Separators for Lithium-Ion Batteries, *ACS Appl. Energy Mater.*, 2023, **6**(7), 3862–3871, DOI: 10.1021/acsaem.2c04170.

42 Y. Xia, X. Li, J. Zhuang, Y. Yuan and W. Wang, Cellulose microspheres enhanced polyvinyl alcohol separator for high-performance lithium-ion batteries, *Carbohydr. Polym.*, 2023, **300**, 120231, DOI: 10.1016/j.carbpol.2022.120231.

43 B. Huang, P. Lai, H. Hua, H. Ma, R. Li, X. Shen, P. Zhang, Y. Zhang and J. Zhao, Application for the porous structure of cellulose separators: Ionic conduction path in lithium-ion battery, *J. Electroanal. Chem.*, 2022, **926**, 116937, DOI: 10.1016/j.jelechem.2022.116937.

44 J. Zhang, Z. Zhang, T. Wu and X. Luo, MOF particles (UiO-66 and UiO-66(Ce))/cellulose nanocomposite separators with regulating ion transport controllably for lithium battery, *J. Electroanal. Chem.*, 2023, **946**, 117708, DOI: 10.1016/j.jelechem.2023.117708.

45 S. Stuckenberg, M. M. Bela, C. T. Lechtenfeld, M. Mense, V. Küpers, T. T. K. Ingber, M. Winter and M. C. Stan, Influence of LiNO3 on the Lithium Metal Deposition Behavior in Carbonate-Based Liquid Electrolytes and on the Electrochemical Performance in Zero-Excess Lithium Metal Batteries, *Small*, 2023, **20**(6), 2305203, DOI: 10.1002/smll.202305203.